

Review

# Shear Stiffening Gels for Intelligent Anti-impact Applications

Chunyu Zhao,<sup>1</sup> Xinglong Gong,<sup>1,\*</sup> Sheng Wang,<sup>1</sup> Wanquan Jiang,<sup>2</sup> and Shouhu Xuan<sup>1,\*</sup>

## SUMMARY

Next-generation intelligent body armor requires high anti-impact performance, low weight, flexibility, and integration with multifunctional wearable devices. Shear stiffening gel (SSG), a kind of high-molecular-weight polymer with interesting properties such as dynamic boron-oxygen (B-O) weak crosslinks, nonlinear mechanical behavior, and high energy dissipation efficiency, has attracted intensive attention from both scientific and industrial sectors. Due to rate-dependent viscoelastic characteristics, SSG has achieved mechanical enhancement following an increase in the external strain rate. Therefore, it is important to understand the viscoelastic behavior of SSG and its derivatives to design the new type of flexible anti-impact devices. This article is a brief review of the recent advances in SSGs, including preparations, mechanical properties, mechanisms, and practical applications in sensors, energy devices, damper controls, and body armors. Finally, the future development potential of SSG as an intelligent anti-impact material is also forecasted.

## INTRODUCTION

The shear stiffening effect, with modulus or viscosity significantly increasing following increases in external strain rates, is a unique phenomenon in polymer materials and fluid suspensions. Materials that exhibit shear stiffening effects are defined as shear stiffening materials.<sup>1–3</sup> The mechanical performance of shear stiffening materials can adapt to the environmental stress field, showing a reversibly sensitive response to external stimuli.<sup>4–6</sup> Presently, there are two common types of shear stiffening materials, shear thickening fluid (STF) systems<sup>7</sup> and shear stiffening gel (SSG) systems,<sup>8</sup> in which the STF is a thick suspension, while the SSG is a gel-like polymer blend (without solvent). As a kind of smart material integrating fast responsiveness, self-healing ability, and stress field adaptability, both the STF and SSG have shown great prospects in terms of impact protection,<sup>9–13</sup> vibration control, and buffering structure.<sup>14–17</sup>

STF as a type of non-Newtonian suspension liquid obtained by dispersing micro- and nano-particles into the polar medium, is the most traditional shear stiffening material and has been extensively researched worldwide. For the STF suspension system, the viscosity decreases with the external shear rate when the strain rate level is relatively low, exhibiting shear thinning characteristics. Once the shear rate reaches a certain critical value, the viscosity of the STF increases rapidly, showing a representative shear thickening effect<sup>18–20</sup> (Figure 1A). Furthermore, the performance of STF is closely related to the dispersed phase particles and dispersion media. There are generally three types of common dispersed phase particles in STF systems. The first type is inorganic mineral particles, such as SiO<sub>2</sub>,<sup>21</sup> CaCO<sub>3</sub>,<sup>22</sup> and

<sup>1</sup>CAS Key Laboratory of Mechanical Behavior and Design of Materials, Department of Modern Mechanics, CAS Center for Excellence in Complex System Mechanics, University of Science and Technology of China, Hefei, Anhui 230027, PR China

<sup>2</sup>Department of Chemistry, University of Science and Technology of China, Hefei, Anhui 230026, PR China

\*Correspondence: [gongxl@ustc.edu.cn](mailto:gongxl@ustc.edu.cn) (X.G.), [xuansh@ustc.edu.cn](mailto:xuansh@ustc.edu.cn) (S.X.)  
<https://doi.org/10.1016/j.xcrp.2020.100266>

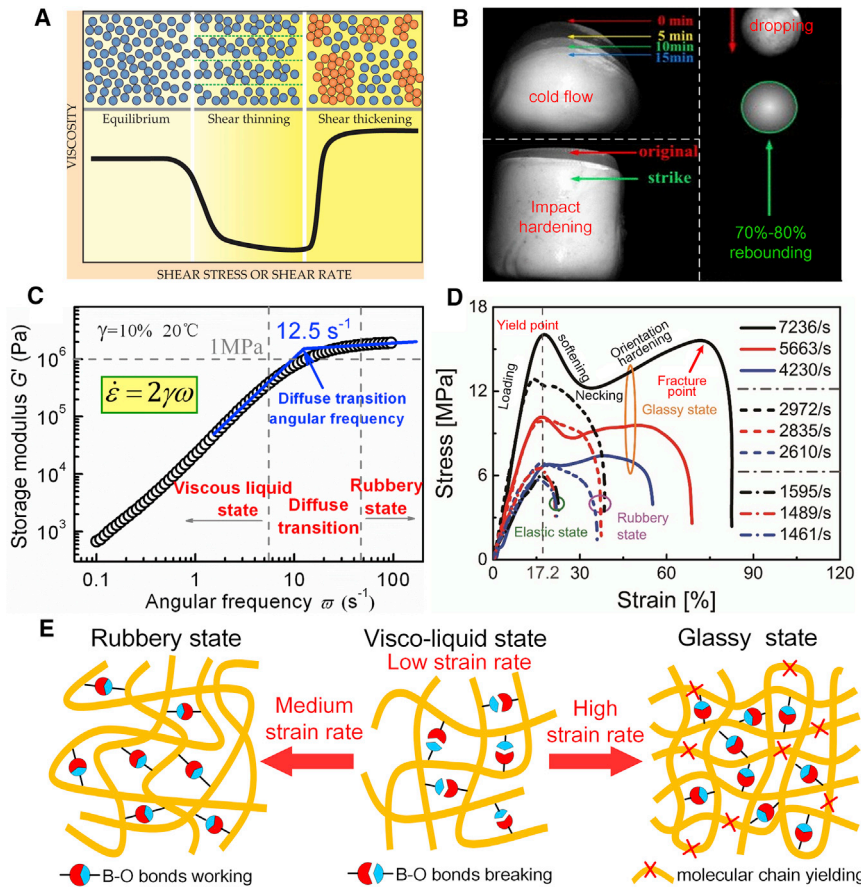


**Figure 1. The Concept of SSG**

(A) Shear thinning and shear thickening in the STF suspension system. Reproduced with permission.<sup>19</sup> Copyright 2009, American Institute of Physics.  
 (B) Cold flow effect of SSG in the natural state and impact hardening phenomenon of SSG under impulsive loading.  
 (C) Transition from viscous-liquid state to rubbery state of SSG. Reproduced with permission.<sup>8</sup> Copyright 2014, American Institute of Physics.  
 (D) The true stress versus true strain for SSG under high strain rate loading. Reproduced with permission.<sup>6</sup> Copyright 2016, Elsevier.  
 (E) Micromechanism among the viscous-liquid state, rubbery state, and glassy state of SSG.

TiO<sub>2</sub>.<sup>23</sup> The second type is variable particles, such as cornstarch particles.<sup>24</sup> The third type is synthetic polymer particles, such as polyvinyl alcohol (PVA),<sup>25</sup> polystyrene acrylonitrile (PS-AN),<sup>26</sup> and polystyrene-ethyl acrylate (PSt-EA).<sup>27</sup> In addition, the common dispersion media are mainly ethylene glycol and polyethylene glycol. Based on the combination of various dispersed phase particles and dispersion media, the STF exhibits different rheological properties in terms of continuous shear thickening (CST)<sup>28,29</sup> and discontinuous shear thickening (DST).<sup>30,31</sup> STF can achieve a phase transition between the liquid-solid state under the actions of an external force. Therefore, STF-based composites have been widely applied to the fields of human body protection,<sup>9,32</sup> safe batteries,<sup>33</sup> and multifunctional composite materials.<sup>34,35</sup> However, the inherent sedimentation and chemical reactivity of STF partly limited their further applications.<sup>6</sup>

SSG, once defined as Silly Putty, is another type of shear stiffening material that has drawn the attention of researchers around the world in recent decades.<sup>8,36,37</sup> In

contrast to the suspension system of STF, SSG is a kind of boron-siloxane polymer silicone rubber with a low crosslinking degree, which is often synthesized using poly-siloxane dimethyl silicone oil or hydroxy silicone oil, boric acid, and benzoyl peroxide (BPO) at high temperature.<sup>38,39</sup> Compared with STF, SSG possesses a larger initial viscosity and more stable performance, making it easier to store and overcome the problems of particle sedimentation and liquid volatilization.<sup>3,40</sup> In the natural state, SSG behaves in a viscoplastic state like plasticine, with typical cold-flow characteristics. Owing to the dynamic boron-oxygen (B-O) weak cross-links, SSG exhibits a typical shear stiffening effect by phase transition among the plastic, elastic, and glassy states with the altering of external loading conditions<sup>8,11</sup> (Figures 1B–1E). Because of the polymer blend character rather than a suspension, this type of material is called SSG, and its mechanical performance is defined as the shear stiffening effect. Interestingly, the rheological properties of SSG is reversible even after it encounters a high-strain rate impact loading.<sup>6,41</sup>

In consideration of this reversible soft-rigid mechanical transforming behavior, SSG shows great potential in damping and shock energy dissipation,<sup>16,17</sup> similar to the STFs. Inspired by the energy absorption behavior of SSG during impulse loading, a series of SSG products have been fabricated for anti-impact devices for military and sports use.<sup>39,42</sup> D3O successfully introduced SSG into polyurethane to provide impact protection for industrial purposes.<sup>43</sup> According to previous reports, SSG could relieve the harmful impact on joints during athletic training while maintaining activity comfort.<sup>42</sup> Using SSG as the filling material, the novel bulletproof helmet provided better security assurance for soldiers in military actions.<sup>11,12</sup> Many studies have indicated that STF/Kevlar was favorable in improving the anti-impact ability and reducing the weight of the body armor by the shear stiffening effect.<sup>11,44</sup> Recently, it was demonstrated that SSG could further enhance the ballistic performance of flexible anti-impact devices without sacrificing wearing comfort.<sup>11–13</sup> Moreover, SSG was also verified to effectively restrict the formation of large Li-branched crystals in a Li battery during the recycling charge-discharge loading process, which successfully suppressed the “shuttle effect” and maintained the integrity of the battery material.<sup>45</sup>

Notably, to make use of its unique rate-dependent behavior and reversible self-healing property, SSG has been applied as a high performance polymer matrix for developing intelligent stretchable devices.<sup>41,46,47</sup> Many conductive fillers such as metallic particles,<sup>48</sup> carbon nanotubes (CNTs),<sup>49,50</sup> graphene,<sup>5,18</sup> and Ag nanowires<sup>46</sup> have been incorporated into SSG to fabricate conductive-SSG composites. The addition of these reinforcement particles not only improved the mechanical performance of SSG but also instantaneously changed the conductive paths in SSG structures according to the microstructural distinctions under different external loadings. Therefore, the external stimulus could be accurately sensed by the change in electric resistance.<sup>50,51</sup> Taking advantage of this mechanoelectric performance, the SSG e-skin,<sup>46</sup> flexible SSG viscoelastic cable,<sup>50</sup> and high-sensitivity SSG monitors<sup>52</sup> have been designed, and these works expanded the potential of SSG in advanced medical equipment and dynamic impact sensing. Very recently, conductive SSGs were also successfully assembled as triboelectric nanogenerators (TENGs) and they could effectively convert the mechanical energy of external loadings into electrical energy.<sup>53–56</sup> By this means, the achieved self-powered ability endowed the SSG-TENG with high potential for flexible battery technologies<sup>45</sup> and portable energy conversion devices.<sup>53</sup>

Overall, it is of great significance to deeply investigate the mechanical behavior and the unique mechanism of SSG to achieve continuous innovations in application

fields. In this review, the recent progress in functional modifications and practical applications of SSGs are summarized based on introductions to preparation methods and mechanical properties. Meanwhile, the challenges in current research are discussed and the prospects of SSG materials are also investigated.

## Preparation and Modulation of SSGs

### *SSGs and Elastic-SSGs*

According to the existing reports, there are two universally acknowledged preparation methods to produce raw boron-siloxane SSG. In the first way, Seetapan et al. prepared SSG by mixing boric acid with hydroxy-terminated polydimethylsiloxane (PDMS) precursors at 120°C for 48 h.<sup>57</sup> According to this method, the final shear stiffening properties of the synthetic SSG materials were strongly affected by the reactant concentration.<sup>58</sup> It was reported that the elastic modulus of SSG primarily decreased and then increased with the molecular weight growth of PDMS precursors. Another method for synthesizing SSG is a more efficient and timesaving method.<sup>3,6,58</sup> First, the boric acid was heated at 160°C for 2 h to obtain pyroboric acid. Second, a proportional simethicone was added to the pyroboric acid to conduct the reaction at the same temperature for 7 h. Finally, by cooling down the mixture to room temperature, the raw SSG was obtained. Using this preparation method, the preparation time for SSG was significantly shortened from 48 to 9 h, while a similar shear stiffening performance was ensured. Hence, SSG could be produced efficiently in large quantities, which guaranteed the production capacity for its application issues.

In general, the mechanical properties of the SSGs are strongly dependent on the network structures of polyborosiloxane. In the natural state, SSG exhibits an obvious cold-flow phenomenon under the gravity effect, which has always been a nonnegligible problem in certain practical conditions.<sup>8,11</sup> It was reported that some specific polymer networks could modify SSGs with good elasticity and mechanical toughness, while the noncovalent B-O interactions in SSGs could be preserved to provide the shear stiffening effect.<sup>59,60</sup> Wang et al.<sup>41</sup> introduced methyl vinyl silicone rubber (VMQ) into SSGs through vulcanization procedures under high temperature and pressure to produce a new type of elastic-SSG. Combining the mechanical properties of SSG and VMQ, the elastomer not only possessed an obvious rate-dependent mechanical response but also the satisfied initial elasticity;<sup>46,56</sup> thus, it exhibited great potential in anti-impact and sensing areas. Similarly, another type of “solid-soft” elastic-SSG was fabricated by polyborosiloxane and PDMS to obtain a double network structure. The covalent crosslinks formed by PDMS provided stable frameworks for polyborosiloxane to overcome fluidity under natural conditions.<sup>60</sup> In addition, the elastic-SSGs also showed outstanding self-healing recyclability against shear failure. Even when rejoining two pieces of cutoff elastic-SSGs without other decorations, the self-healed elastic-SSGs exhibited similar mechanical properties to the original elastic-SSGs.<sup>41,59</sup> Due to its high stretchability, flexibility strain-rate sensitivity, and shape-recovery ability, the burgeoning elastic-SSG is believed to be an ideal candidate for smart flexible devices in the area of anti-impact.

### *Multifunctional Composites Based on SSGs*

The mechanical properties of the composite could be effectively controlled by introducing functional fillers.<sup>61–63</sup> Hence, it was shown that the mechanical behavior of the SSG could also be directionally controlled by reinforcing phase particles. For example, the shear storage modulus of the SSG increased with CaCO<sub>3</sub> doping via the particle enhancement effect.<sup>8,11</sup> More important, many additive fillers possess unique electromagnetic responses, which endow the SSGs with multifunctionalities

in a wide range of applications. Here, the SSG polymer had a brilliant ability to coexist with some reinforcing particles such as magnetic powders and conductive medium.<sup>48,52</sup> Basically, the overall mechanical performance of SSG was improved due to the addition of functional particles.<sup>6,51</sup> The SSG is a kind of polymer gel with good chemical inertness; therefore, it overcomes the particle sedimentation problem often found in STFs and maintains long-term stability.<sup>39,42</sup>

A series of high-performance SSGs with magnetically tunable rheological properties were fabricated by introducing magnetic fillers into the SSG matrix. The mechanical tests indicated that the hybrid method could endow the SSG with both a shear stiffening effect and a high magneto-sensitive effect.<sup>64–67</sup> The magnetic-SSGs were first prepared by using the carbonyl iron particles (CIPs) and  $\text{Fe}_3\text{O}_4$  particles as the additives. In contrast to the pure SSG, the magnetic-SSG had a larger initial storage modulus, and the relative shear stiffening performance was also improved by applying an external magnetic field. Moreover, the soft magnetic CIPs were proven to have a stronger enhancement than that of hard magnetic particles<sup>3,48</sup> (Figures 2A and 2B). Based on this discovery, a magnetic susceptibility elastic-SSG with better stretchability was further designed, and a linear magnetic dependence of the relative storage modulus was observed (Figure 2C). In addition, the shear stiffening performance of magnetorheological elastic-SSG could also be controlled by the mass fraction of magnetic particles<sup>41</sup> (Figure 2D). Interestingly, a unique thermal self-healing property was observed in magnetorheological elastic SSG, in which the recovery effect enabled the chapped samples to be connected together<sup>41</sup> (Figure 2E). Golinelli et al. also proposed that Fe-Co-Ni nanowires were another feasible additive to fabricate magnetic-SSG.<sup>68</sup> The magnetic particles in the composites aligned to form a catenulate structure in response to the magnetic field and led to an increase in the storage modulus<sup>69</sup> (Figure 2F). To investigate the mechanical behavior of magnetic-SSGs at high strain rates, an impact test machine was used to analyze the influence of experimental parameters on the magnetorheological effect of magnetic-SSG.<sup>70</sup> In particular, using a modified split-Hopkinson pressure bar (SHPB) system,<sup>6</sup> it was found the magnetic-SSG entered a glassy state when the strain rate reached  $7,236 \text{ s}^{-1}$ , which further demonstrated the rubbery-glassy transition of magnetic-SSG at a high strain rate. In addition, according to the experimental results, a qualitative explanation was illustrated to describe the strengthening effect based on magnetic dipole theory.<sup>69</sup>

The addition of high-performance conductive particles into SSG is another strategy to prepare bifunctional SSG with improved mechanical behaviors such as elastic modulus, yield stress, and strength. More important, the conductivity of SSG was significantly improved; thus, it showed great potential in dynamic mechanoelectric coupling applications. To investigate the mechanoelectric coupling effect of conductive-SSG, a series of conductive fillers, such as CNTs,<sup>49–51</sup> carbon black,<sup>13,42</sup> Ag nanowires (AgNWs),<sup>46,59</sup> and graphene sheets<sup>52,63</sup> were added to the SSG by mechanical mixing or solution mixing methods (Figure 3A). The conductive additives were proven to be evenly dispersed within SSG due to macromolecule construction and thus resulted in stable initial resistance under the natural state.<sup>13,42</sup> Once suffering impact loadings, the inner structure of the conductive paths of SSG experienced temporary damage, and the redistribution of conductive particles dominated the change in conductivity (Figure 3B).<sup>50</sup> Evidenced by the low percolation threshold, the conductive-SSG was recognized as a new type of high-performance conductive gel system (Figure 3C).<sup>51</sup> The investigation of the mechanoelectric coupling performance illustrated that the conductive carbon black additive not only improved the rheological properties but also decreased the creep effect of

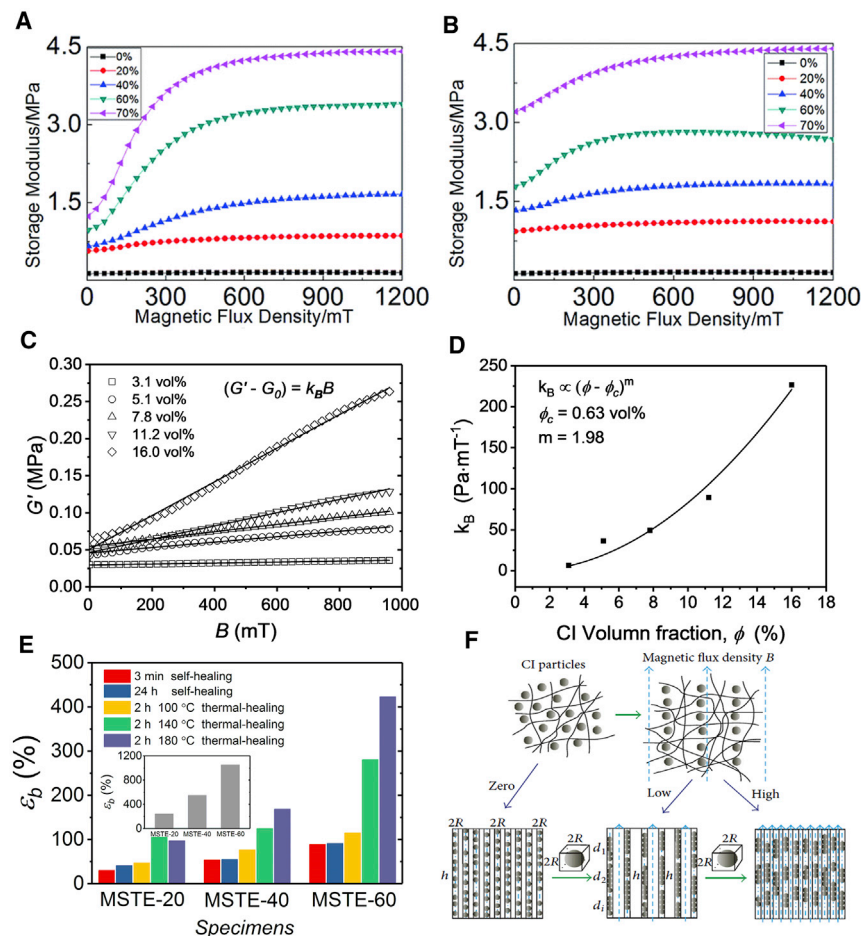


**Figure 2. The Mechanical Enhancement Effect of Magnetic Particles on SSGs**

(A and B) Storage modulus of magnetic SSG-CIPs (A) and SSG-Fe<sub>3</sub>O<sub>4</sub> (B). Reproduced with permission.<sup>3</sup> Copyright 2014, Royal Society of Chemistry.

(C) Relationships between the storage modulus and magnetic flux density of magnetorheological elastic-SSG.

(D) Influence of volume fraction of magnetic particles on magnetorheological elastic-SSG.

(E) Self-healing performance with thermal treatments of magnetorheological elastic-SSG.

Reproduced with permission.<sup>41</sup> Copyright 2018, Elsevier.

(F) Chain-formation mechanism for magnetic SSG and the nonperforative particle aggregated chains model. Reproduced with permission.<sup>69</sup> Copyright 2018, Hindawi.

SSG<sup>42</sup> (Figure 3D). Moreover, the change in the resistance showed linear relationships upon mechanical stimuli, which endowed the final product with great potential in the sensing area<sup>42,52,63</sup> (Figure 3E). All of the studies indicated that the electric performance of conductive-SSG was influenced by external loading. Therefore, the SSG was proposed to be feasible in developing the next-generation sensing devices due to the mechanoelectric coupling performance.

### Rate-Dependent Mechanical Behavior of SSGs

#### Shear Stiffening Performance of SSG

To fully understand the mechanical properties of SSGs, both experimental and theoretical methods were explored. With the assistance of rheological measurements, the storage modulus of SSG in the natural state was found to be 10<sup>2</sup> Pa, leading to a completely viscous character (Figure 4A). Different from the STF with the initial

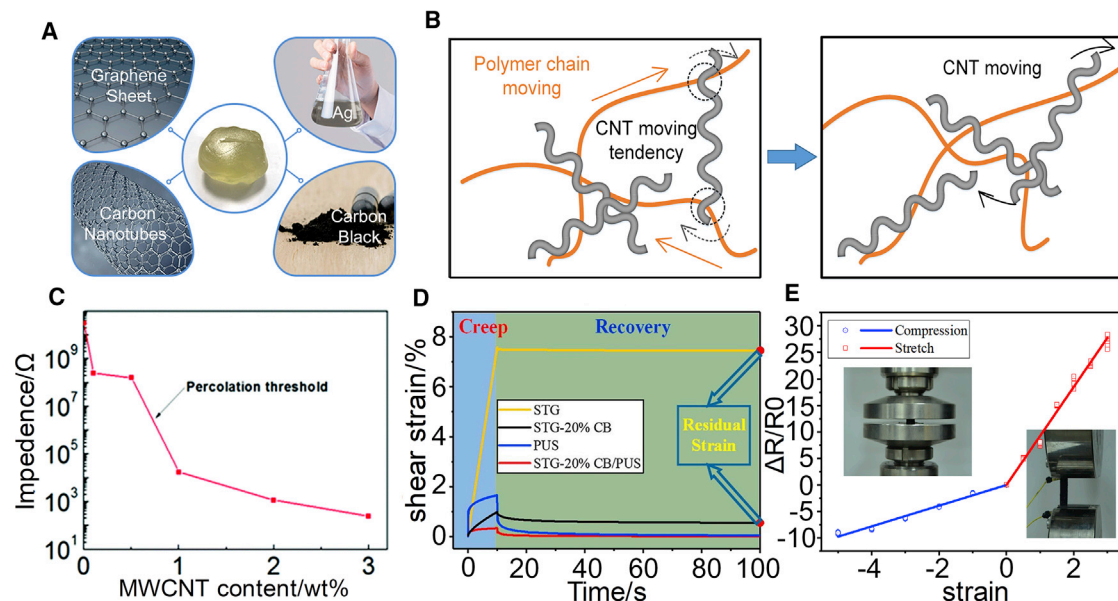


**Figure 3. The Mechanoelectric Coupling Effect of Conductive SSGs**

(A) Conductive medium used to prepare conductive-SSG.

(B) Evolution of conductive network for conductive-SSG under external stimuli. Reproduced with permission.<sup>50</sup> Copyright 2019, Royal Society of Chemistry.

(C) Impedance percolation threshold of CNTs/SSG. Reproduced with permission.<sup>51</sup> Copyright 2015, Royal Society of Chemistry.

(D) Creep and recovery behavior of conductive-SSG under shear stress.

(E) Linear dependence of resistance under compression and stretch loadings. Reproduced with permission.<sup>42</sup> Copyright 2018, Elsevier.

modulus of  $\sim 10^{-1}$  Pa, the viscous SSG displayed a more stable structure in the natural state.<sup>47,63,71</sup> However, the stiffness of SSG rapidly improved as the external strain rates increased to the critical value.<sup>11,37,42</sup> When this viscoelastic transition was processed, a cross-point between the storage modulus ( $G'$ ) and loss modulus ( $G''$ ) was displayed in the frequency sweeping curve.<sup>16,52,72</sup> The viscous state dominated the material behavior under the low-frequency region when  $G'$  was less than  $G''$ . However, once  $G'$  exceeded  $G''$  after the cross-point, the shear stiffening phenomenon appeared and the SSG showed high-elastic behavior. In this case, the storage modulus of SSG reached as high as  $10^6$  Pa, which far exceeded the STF of  $10^2$  Pa<sup>47,71</sup> (Figure 4B). The high strain rate stress-strain relationship of  $\text{CaCO}_3$  particle-reinforced SSG was studied by using SHPB technology with a strain rate of up to  $14,132 \text{ s}^{-1}$ . Different from the viscoelastic behavior at low strain rates, an elastic-glassy transition appeared. Under this condition, the SSG displayed higher strength and obvious brittleness, with the maximum storage modulus approaching  $10^8 \text{ Pa}$ <sup>8</sup> (Figure 4C).

The theoretical analysis through viscoelastic constitutive models was another method to study the shear stiffening behavior of SSG. Cross et al.<sup>36,73</sup> proposed a standard linear solid (SLS) model by combining a spring element in series with a classical Maxwell element and successfully explained the basic viscoelastic behavior of SSG. To better clarify the creep effect of SSG, a modified SLS model by adding another series of Maxwell elements<sup>41</sup> was proposed, and the model demonstrated good consistency with the experimental results (Figure 4D). Moreover, Goertz et al.<sup>74</sup> also used a ternary Maxwell parallel element model to investigate the influence of temperature on the rheological properties of SSG, and the time-temperature equivalence in SSG system could be clearly explained.

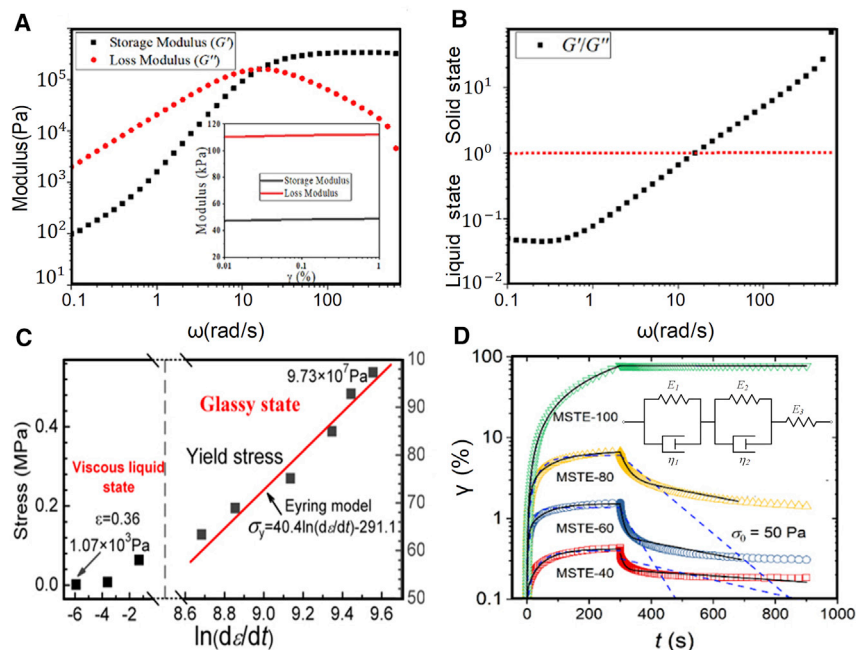


**Figure 4. The Mechanical Response of SSGs under Different Strain Rates**

(A) Rheology property during frequency sweeping.

(B) Criterion for shear stiffening. Reproduced with permission.<sup>47</sup> Copyright 2020, Elsevier.

(C) Yield stress under different strain rate. Reproduced with permission.<sup>8</sup> Copyright 2014, American Institute of Physics.

(D) Strain curves of magnetic elastic-SSGs in the creep measurements and modified SLS model. Reproduced with permission.<sup>41</sup> Copyright 2018, Elsevier.

### Microscopic Shear Stiffening Mechanism

The SSG is a kind of boron-siloxane polymer silicone rubber, and the shear stiffening effect originates from the dynamic B-O crosslinking ligands. Obviously, the electrons on p-orbital from the B atom were easy to escape, while there were plenty of free electrons in the O atom (Figure 5A). Therefore, the weak electron cloud interactions between B and O atoms could be assembled by sharing electrons<sup>42,51,75</sup> (Figure 5B). The Fourier transform infrared spectroscopy (FTIR) techniques<sup>58,76–78</sup> were used to analyze the microscopic shear stiffening effect. Typically, the stretching vibrations of Si-CH<sub>3</sub> (1,257 cm<sup>-1</sup>), Si-O (1,015 cm<sup>-1</sup>), Si-O-B (892 cm<sup>-1</sup> and 862 cm<sup>-1</sup>) and B-O (1336 cm<sup>-1</sup>) were obtained in the SSG (Figure 5C). In general, the current explanations for shear stiffening mechanism were mainly based on the dynamic evolution of B-O crosslinks through unique breaking and recovering behaviors.<sup>12</sup> Under low strain rate external loadings, the corresponding timescale for molecular chain motion was relatively large. The B-O bonds had enough time to be broken, and the damping force caused by the entanglement of molecular chains was the main obstacle to molecular deformation. Hence, the SSG exhibited viscosity characteristics with flowability at the macroscale.<sup>45,60</sup> However, as the strain rate grew to a higher level, the timescale for molecular motions became much shorter than the characteristic breakage time of B-O crosslinks. In this case, the unbroken B-O bonds generated more resistance against the movement of molecular chains. The molecular chains were too hard to untangle, and the rotation of the chain segments dominated the mechanical property of the SSG, which resulted in the high-stiffness state at the macroscale.<sup>38,73,74</sup> In addition, there was also a transition region between the elastic state and the glassy state observed at a higher strain rate. At the



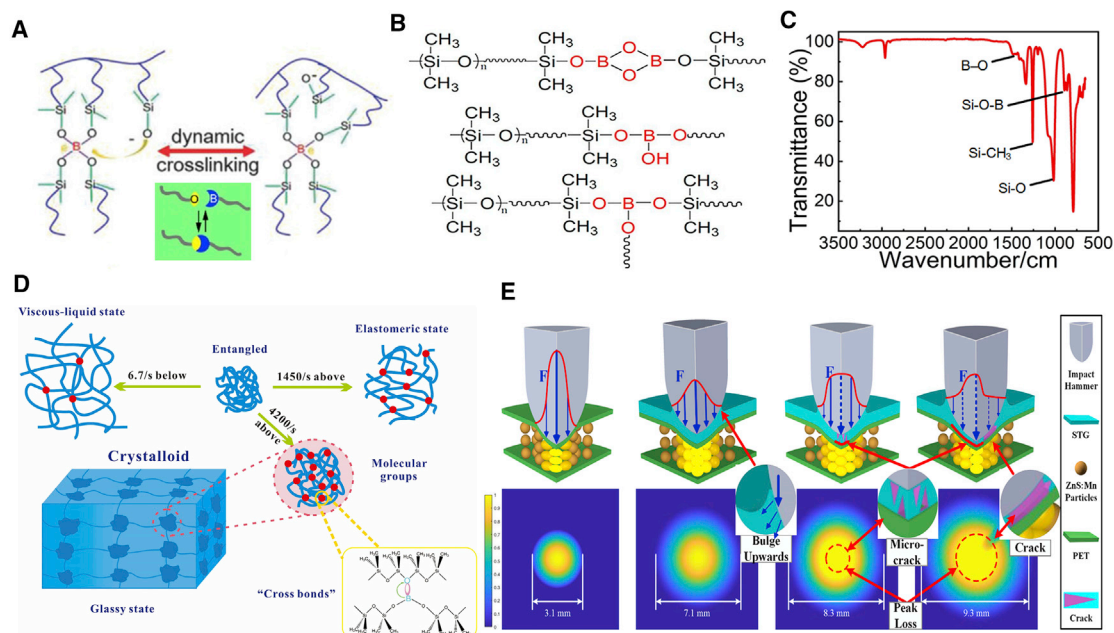


**Figure 5. The Mechanism of Shear Stiffening Phenomenon**

(A) Crosslink-forming process of B-O dynamic bonds. Reproduced with permission.<sup>45,60</sup> Copyright 2018, Wiley-VCH Verlag; Copyright 2019, American Chemical Society.

(B) Possible structure of B-O dynamic bonds. Reproduced with permission.<sup>42</sup> Copyright 2018, Elsevier.

(C) FTIR spectrum of SSGs. Reproduced with permission.<sup>12</sup> Copyright 2019, IOP Publishing.

(D) Explanations for state transition process. Reproduced with permission.<sup>6</sup> Copyright 2016, Elsevier.

(E) Energy dissipation mechanism under impact loading. Reproduced with permission.<sup>47</sup> Copyright 2020, Elsevier.

critical point, all of the crosslinks were disabled to be disentangled in the loading section and broke easily.<sup>6</sup> Therefore, the stress reached the yield point and led to fracture failure for the overall structure (Figure 5D). Importantly, the broken dynamic B-O bonds could be recombined once B and O atoms were close to each other after the reloading period, and this interesting phenomenon was responsible for the novel self-healing performance of SSG.<sup>79</sup>

Recently, the mechanism of SSG under impact stimuli was further characterized by using a mechanoluminescence method. On account of additional ZnS:Mn particles, the invisible mechanical response was converted into visible light signals.<sup>47</sup> The change in light intensity during the impact process originated from the microcrack extension in the internal structure of the SSG. Under these circumstances, the microcracks dissipated a large amount of impact energy before the failure of SSG, which resulted in the weakness of light intensity (Figure 5E). Meanwhile, the elastic state of SSG effectively decreased the stress concentration. As a result, both the shear stiffening and fracture failure were recognized as the main mechanism responsible for the anti-impact properties of SSGs.

### SSG Composites with Anti-impact Performance

#### SSG Composites Strengthened by Porous Matrices

SSGs were favorable for constructing anti-impact composites due to their outstanding shear stiffening effect at high strain rates. Using the good cushioning characteristics of the porous structure, the SSG was added into the porous matrix to further improve its energy absorption performance. In consideration of the low viscosity under a low strain rate, the SSG could be easily integrated into the porous

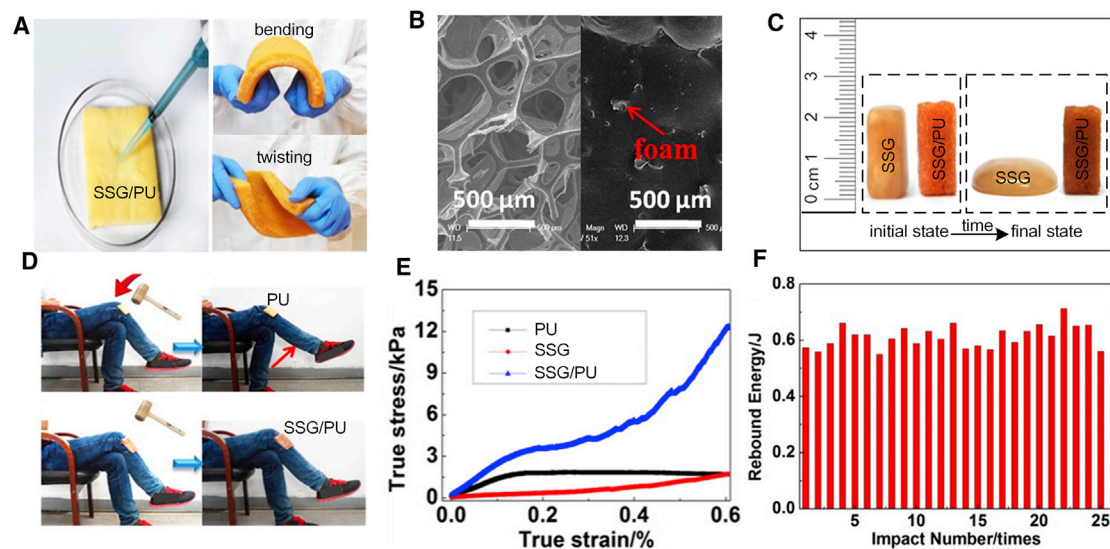


**Figure 6. The Design of SSG/PU Composite Structure.**

(A) Preparation method of SSG/PU and basic physical properties.

(B) SEM comparison between neat PU and SSG/PU.

(C) Improvement of the cold-flow effect of SSG/PU compared to pure PU.

(D) Comparison of the knee jump effect under impact between the SSG suffer and the SSG/PU suffer.

(E) Stress-strain curves among SSG, PU, and SSG/PU.

(F) Reliability of rebound energy versus cyclic loading impact.

Reproduced with permission.<sup>39</sup> Copyright 2016, American Chemical Society.

matrix to form a stable structure. Polyurethane (PU) sponge was first used to carry SSGs<sup>39</sup> (Figure 6A). Scanning electron microscopy (SEM) imaging illustrated that the SSG filled within the holes of porous PU<sup>60</sup> (Figure 6B). The initial storage modulus of the SSG/PU composite improved over 10 times that of pure foam, which further enhanced the stretchability and reduced the cold-flow drawbacks of the SSG (Figure 6C). Because of the large stretchability and elastic deformation, the SSG/PU showed reduced irrecoverable strain.<sup>39,42</sup> Specifically, as a type of high-performance elastic structure, a creative attempt was made to use the unique mechanical behavior of SSG/PU during impact loading. Compared to the traditional PU, the knee jump reflexing level was effectively decreased using SSG/PU as the buffer layer<sup>14</sup> (Figure 6D). Meanwhile, influenced by the shear stiffening effect at higher strain rates, the stiffness of SSG/PU obviously improved<sup>78</sup> (Figure 6E). Hence, during the impact loadings, the overall elastic deformation of SSG/PU was generated to disperse the energy in the central contact area, and most of the impact energy was converted into elastic reversible energy during the unloading process. Benefiting from the structural controlling strategy, the SSG/PU composite not only achieved better strength against impulsive loading but also possessed fatigue resistance performance, which ensured the mechanical stability under cyclic utilization<sup>39,42</sup> (Figure 6F). In addition, other porous structures such as elastic polymer polyurea-urethane (PUU) were also reported to modify the SSG structure with high stretchability and long-term stability, which expanded the structural optimization method for SSGs.<sup>79</sup>

### SSG/Kevlar Fabric Composites

The SSG could be also introduced into fabrics to reinforce their anti-impact performance. Compared with other ordinary organic fabrics, Kevlar showed high tensile strength, high tensile modulus, and low break elongation; thus, it has been widely

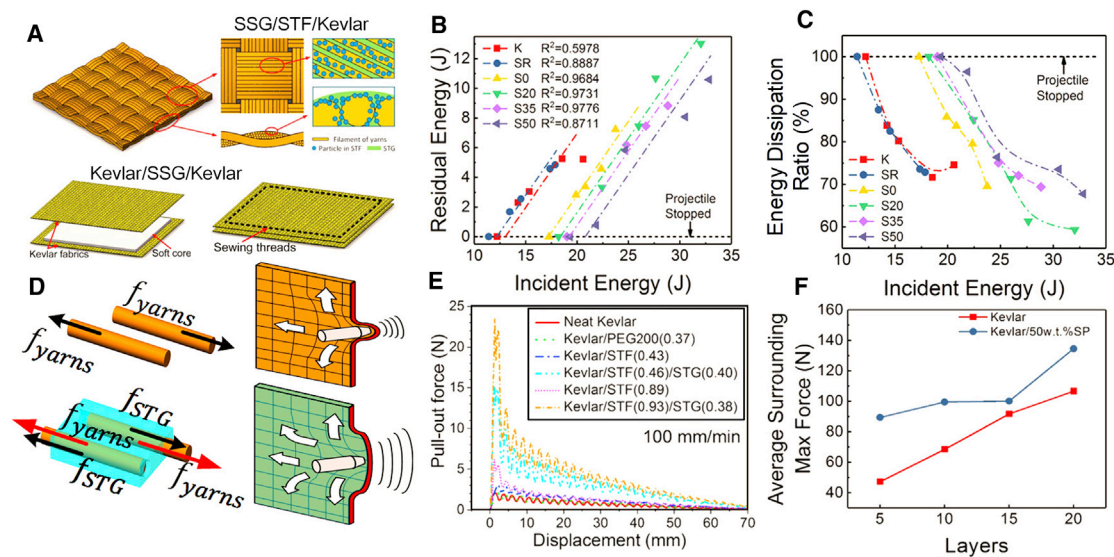


**Figure 7. The Anti-impact Performance of SSG/Kevlar Composite**

(A) Preparation method for SSG/STF/Kevlar and Kevlar/SSG/Kevlar. Reproduced with permission.<sup>11,44</sup> Copyright 2017 and 2018, Elsevier.  
 (B) Residual kinetic energy of the projectile at different incident energy for Kevlar/SSG/Kevlar.  
 (C) Residual kinetic energy of projectiles during ballistic testing for Kevlar/SSG/Kevlar. Reproduced with permission.<sup>11</sup> Copyright 2017, Elsevier.  
 (D) Friction enhancement mechanism for SSG/Kevlar composites. Reproduced with permission.<sup>12</sup> Copyright 2019, IOP Publishing.  
 (E) Comparison of yarn pull-out force for neat Kevlar, Kevlar/STF, and Kevlar/STF/SSG. Reproduced with permission.<sup>44</sup> Copyright 2018, Elsevier.  
 (F) Stress dissipation effect of multilayer neat Kevlar and SSG/Kevlar under ballistic impact. Reproduced with permission.<sup>12</sup> Copyright 2019, IOP Publishing.

used as a basic material in soft body armors.<sup>80,81</sup> Different from Kevlar composites such as Kevlar/epoxy<sup>82</sup> and Kevlar/ceramic,<sup>83</sup> the flexible Kevlar composites with satisfied ballistic behavior<sup>84</sup> have attracted increasing research interest.<sup>84</sup> Recently, STF/Kevlar composite fabric was successfully developed as a novel kind of “liquid armor.” Various efforts have been conducted to construct high-performance STF/Kevlar body armor and investigate the real shear-thickening anti-impact mechanism. However, the fluidic nature and weak stability partly limited their further application. In consideration of the good shear stiffening effect and chemical stability, the SSG was proposed to be a potential candidate to substrate the STF in the next-generation body armor.

The SSGs have been integrated into Kevlar fabric toward flexible anti-impact body armors by two preparation methods (Figure 7A). The first method was the “dissolution-volatilizing” method, in which the SSG was immersed into the gaps of bullet-proof Kevlar fabrics using a diluted SSG using the organic solvents such as ethyl alcohol and acetone to dilute the SSG.<sup>49</sup> Second, the SSG was found to be easily combined with Kevlar fabrics through a simple “mechanical packing” method, with a pure SSG layer sandwiched by two Kevlar pieces. As a high-performance fabric composite, the SSG/Kevlar possessed an outstanding anti-impact effect compared to the traditional flexible protective material<sup>11</sup> (Figures 7B and 7C). During the shear stiffening process, the friction of fibers significantly increased with the filling of SSG. Hence, SSG/Kevlar showed greater resistance against the penetration impact than the neat fabric<sup>12</sup> (Figure 7D). With combinations of anti-impact characteristics originating from the structural advantages of Kevlar fabrics and the enhancement effects of SSG, the attenuation of the impact center force for SSG/Kevlar under high strain-rate loading was up to 64.1%, which was much larger than the neat Kevlar.<sup>12</sup> Moreover, the STF/SSG/Kevlar composite can be further developed.

As a result of the synergistic shear stiffening effect of both SSG and STF, the composite displayed better stab resistance properties, as proven by yarn pull-out testing<sup>44</sup> (Figure 7E). In addition, anti-impact tests were conducted and both the effective energy dissipating and stress concentration weakening phenomenon were found in the SSG/Kevlar, which further explained the high stability of the SSG/Kevlar structure (Figure 7F). Moreover, by introducing reinforcement particles such as CaCO<sub>3</sub> and carbon black into SSG, the modified SSG/Kevlar could decrease the impact force and achieve a lower ballistic limit velocity value ( $V_{50}$ ) according to the results of fragment simulated penetration (FSP) tests.<sup>11,13</sup> Based on the above analysis, it can be concluded that the SSG/Kevlar composites would be attractive for designing the flexible body armors.

### Applications of SSGs

Based on the above-mentioned discussions, it can be found that the SSGs not only achieved satisfactory shear stiffening effects but could also sensitively respond to the applied stress fields. Meanwhile, with the decorations of specific dopant particles, the multifunctional SSGs with additional magnetic responses, electrical signal feedbacks, and excellent self-healing properties are also achieved. Therefore, a series of investigations have been conducted to explore the SSGs in the fields of vibration controls, sensors, energy devices, body armors, and triboelectric nanogenerators.

#### SSG Dampers

Similar to the STF, the SSG can be used in damper due to its unique shear stiffening effect. The shock transmission unit (STU) is an innovative attempt for damper devices to fill SSGs. Because of the different rheological responses to the external stress fields, the SSG provided ease of movement for the STU under a lower external force. However, once suffering from impact loadings, the STU achieved a rigid link and restricted the movement of the piston in the phase transition process. In addition, the SSG-based STU could provide greater damping force than the STF damper because of its higher viscosity in the shear stiffening process.<sup>16</sup> Due to the sensitive mechanical properties under an external magnetic field, the magnetorheological SSG further broadened the semiactive controlling characteristics for the damping controls. In addition to the fast response of the speed locking function under external impact excitations, the damping force of the magnetorheological SSG damper could be accurately controlled by the applied magnetic field according to a multiparameter and symmetry hysteretic model.<sup>17</sup>

#### SSG Sensors

The above-mentioned conductive SSG was considered to be an excellent candidate for designing sensors because of its good flexibility and conductivity. The piezoresistive-type conductive polymer composites, often fabricated by polymer matrices and conductive nanofillers, enable the transitions from loading signals into electrical signals. Because of the easy preparation method and high sensitivity, this type of sensor showed application prospects in terms of dynamic sensing.<sup>46</sup> In addition, owing to the shear stiffening anti-impact function of the SSG, the SSG sensors could resist impact loadings, which were demonstrated to be superior to the traditional piezoresistive-type sensors.<sup>39,49</sup> The most original SSG sensor was produced by mixing conductive CNT particles into SSGs, and it could dynamically control the intensity of a light-emitting diode (LED) bulb with a fast response against external loading. Once the conductive composite was struck, the intensity of the LED bulb decreased clearly due to the sharp interruptions of conductive networks originating from the shear stiffening effect (Figure 8A).<sup>51</sup>

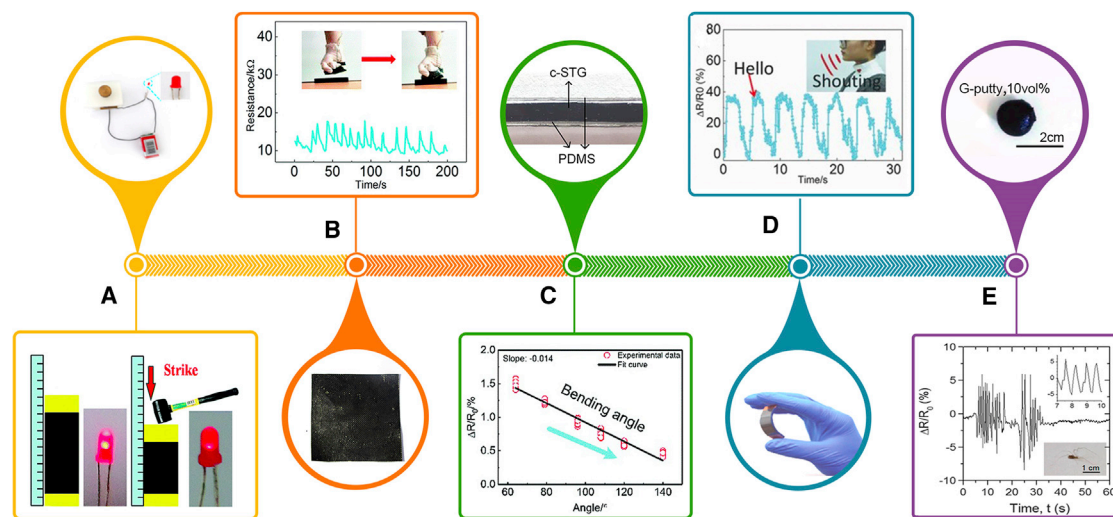


**Figure 8. Sensing Applications of SSG Composites**

(A) First-generation conductive-SSG resistance adjustment devices. Reproduced with permission.<sup>51</sup> Copyright 2015, Royal Society of Chemistry.  
 (B) Conductive-SSG/Kevlar and response against human paces and fist loading. Reproduced with permission.<sup>49</sup> Copyright 2017, Royal Society of Chemistry.  
 (C) Conductive-SSG@PDMS cable and the sensing ability to bending deformation at different angles. Reproduced with permission.<sup>50</sup> Copyright 2019, Royal Society of Chemistry.  
 (D) Tactile and acoustic perception behavior of SSG e-skin. Reproduced with permission.<sup>46</sup> Copyright 2018, Wiley-VCH Verlag.  
 (E) Resistance change associated with a spider walking on graphene/SSG. Reproduced with permission.<sup>52</sup> Copyright 2016, American Association for the Advancement of Science.

The conductive-SSG could also be attached on the flexible matrix to form reusable sensing devices. The movements of human paces and fist loadings were successfully monitored by the conductive SSG fabrics (Figure 8B). Recently, a flexible viscoelastic coupling cable with the wire-like CNT doped conductive-SSG encapsulated within a PDMS shell was reported. Different from the plastic conductive SSG with a cold-flow nature, the conductive-SSG@PDMS sensor was sensitive to external stimuli and the sensitivity showed an interesting self-adopting manner. Thus, it could attach to the nonflat surface to simultaneously monitor body actions<sup>50</sup> (Figure 8C). Moreover, the conductive SSG could also fill within the PU sponge to design the high-performance strain sensor. The conductivity of SSG/PU varied quickly and maintained stability up to 45 cycles of compression and stretch loadings.

Furthermore, the conductive SSG could simultaneously improve the mechanical performance of sensors. The conductive SSG strain sensor could sensitively detect the impact stimulus from 0.147 to 1450 mJ and decrease the attacking force by 63% simultaneously.<sup>39</sup> Recently, the increasing demand for ultrahigh sensitivity sensing devices further promoted the development of SSG-based sensors. It was reported that a new generation of multifunctional e-skin was created by assembling elastic-SSGs, AgNWs, and polyester film (PET film) together. Different from the above-mentioned sensors, the e-skin possessed excellent sensing characteristics, which could be used to distinguish tiny activities such as light touch, stroking, and even talking<sup>46</sup> (Figure 8D). Analogously, Boland et al.<sup>52</sup> designed an ultrasensitive sensor by doping graphene into the SSG. The graphene/SSG composites exhibited unusual electromechanical behavior, such as special post-deformation temporal relaxation of resistivity and nonmonotonic strain-dependent conductivity, which was associated with the mobility of the graphene in the low-viscous SSG matrix. More important, the addition of graphene produced extremely sensitive resistance changes

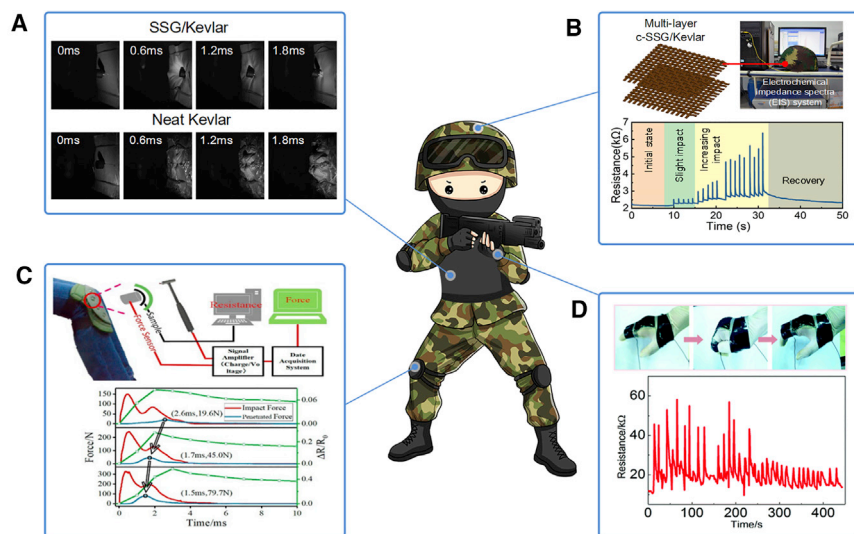


**Figure 9. Safeguarding Applications of SSG Composite**

(A) Comparison of bulletproof material fabricated by SSG/Kevlar and neat Kevlar. Reproduced with permission.<sup>12</sup> Copyright 2019, IOP Publishing.

(B) Conductive-SSG/Kevlar hamlet and the resistance responses under multiple hammer impact. Reproduced with permission.<sup>13</sup> Copyright 2019, Elsevier.

(C) Anti-impact and dynamic sensing performance of conductive-SSG kneepad. Reproduced with permission.<sup>42</sup> Copyright 2018, Elsevier.

(D) Mechanoelectric performance of a hand protection device. Reproduced with permission.<sup>49</sup> Copyright 2017, Royal Society of Chemistry.

The illustration of the soldier in the center was reproduced with permission from <https://699pic.com>.

under slight stress stimuli, such as finger swing, breathing, pulse beating, and even the step moving of a spider<sup>52</sup> (Figure 8E).

### SSG Anti-impact Devices

As a smart material with shear stiffening performance, SSGs have been widely used to produce next-generation anti-impact devices. Based on the investigation of the low-velocity impact response of sandwich panels with SSG cores, it is found that the SSG sandwich structure led to larger energy absorption compared to panels with other cores, such as chloroprene rubber and ethylene-propylene-diene monomer.<sup>37</sup> To fabricate flexible anti-impact body armor, a lightweight SSG/Kevlar protection device was successfully created. Different from the ballistic behavior of neat Kevlar fabrics, the SSG/Kevlar structure showed better performance in stress dispersion and energy dissipation. Moreover, only smaller topography failures were observed in SSG/Kevlar, which indicated that the hybrid structure was optimum for bulletproof materials<sup>12</sup> (Figure 9A). Moreover, by combining the excellent anti-impact characteristics and dynamic sensing performance of conductive SSG fabrics, several flexible anti-impact sensing devices were designed. The conductive-SSG/Kevlar fabric was attached to the surface of a commercial helmet to manufacture an electronic helmet that could both resist and detect the impact simultaneously during the penetration process. With the optimized proportion of carbon black and SSG, the helmet could not only maintain the mechanical stability under multiple impact loadings but also precisely monitor the damage evolution<sup>13</sup> (Figure 9B).

In addition, an anti-impact and sensing bifunctional kneepad was developed by replacing the middle part of the inner cushion with a conductive carbon black/SSG/PU sponge. The modified kneepad traced the basic motion of humans within an

extremely short response time of 3 ms and decreased the impact force by >40% compared to the original kneepad. In this case, the smart kneepad could be widely used in sports protection and signal feedback for athlete training<sup>42</sup> (Figure 9C). Moreover, the conductive SSG also could be applied in dynamic hand protection with physical combinations of bulletproof fabrics<sup>49</sup> (Figure 9D). With the outstanding flexible safeguarding performance and fast self-feedback response to external loading, wearable anti-impact hand protection devices also showed promising prospects in security actions.

### SSG TENGs

To further develop lightweight flexible electronic devices based on SSG composites, the self-powered TENG has attracted universal attention in shear stiffening safeguarding materials.<sup>85–87</sup> Based on the triboelectric effect and electrostatic induction, the TENG could convert mechanical energy into electric energy as a green and sustainable power source. To date, the modification of TENGs with the ability to withstand large strains and avoid failure under impulsive loadings has been a hotspot in current research. Inspired by the kinetic energy harvesting properties of TENGs and the excellent electric-mechanical coupling effect of conductive SSGs, a multifunctional self-powered force sensing TENG composites was successfully developed by encapsulating liquid metal GalSn into the structure of SSG/PDMS<sup>53,56</sup> (Figure 10A). Due to the friction electrification and electrostatic induction effects of the SSG/TENG, the external kinetic energy could be converted into electrical energy during the loading process.<sup>56</sup> The output voltage or current was proven to increase in accordance with the improvement of loading force and frequency within a certain range (Figures 10B and 10C). Moreover, the output voltage and maximum output power of the TENG with a size of 50 × 50 × 4 mm<sup>3</sup> were 35.72 V and 182.17 μW under a compression frequency of 10 Hz (Figure 10D). Interestingly, benefitting from the high stretchability, flexibility, and sensitivity of SSG, the TENG could also be used as a self-powered sensor to monitor different human movements. To further improve the triboelectric performance of SSG/TENG, polytetrafluoroethylene (PTFE) was introduced as an electrode component.<sup>53</sup> The modified PTFE/SSG/TENG displayed a larger output voltage (44.20 V) and maximum power (390.73 μW).

In addition, a wearable electronic skin array was made up of the PTFE/SSG/TENG. The electronic skin transformed the external impact energy into electrical energy while possessing excellent sensing performance, which could be verified by a force distribution map in different impact regions (Figures 10E–10G). Very recently, assembled by magnetorheological SSE, Cu foil, and metal wires, a magnetically sensitive TENG with tunable electric–mechanical performance was reported.<sup>54</sup> Using simple testing equipment, the electric property of the TENG was found to be remarkably controlled by the magnetic field (Figures 10H and 10I). The output voltages for the TENG showed an almost linear positive correlation with the external pressures, and the slopes of all of the fitted curves represented the sensitivity to loading forces, which ensured sensing accuracy for the applications of the TENG (Figure 10J). In addition, a CNT-SSG electrode was reported to endow the TENG with the outstanding capability of adapting to different irregular surfaces and instantaneous healing from mechanical damage. Meanwhile, the output property was also improved due to the more effective contact electrification and introduced cation dopants, which provided a power supply to soft electronics and robotics.<sup>55</sup>

### Conclusions and Perspectives

The SSG and its derivatives possessed wonderful characteristics, such as shear stiffening, multifield response, self-adaptive ability, and self-healing properties. Thus, they attracted increasing interest during the past decade. Based on the in-depth

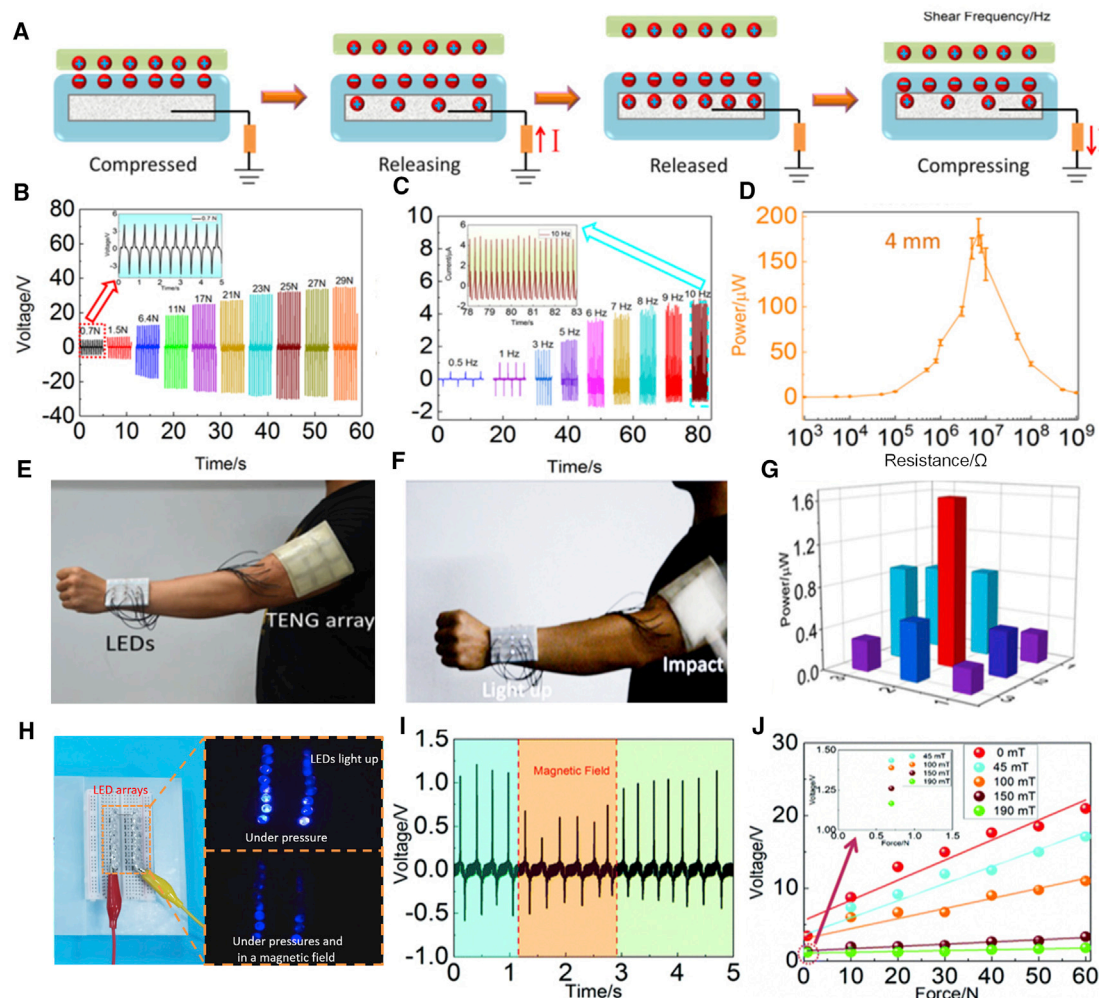


**Figure 10. High-Performance SSG/TENG Composite**

(A) Electricity generation process of SSG/TENG.

(B) Generated output voltage of liquid metal-based SSG/TENG under various applied forces.

(C) Generated current of liquid metal-based SSG/TENG under various frequencies.

(D) The electric power output of 4 mm liquid metal-based SSG/TENG at 500 M $\Omega$ . Reproduced with permission.<sup>56</sup> Copyright 2018, Elsevier.

(E and F) SSG/TENG array acts as wearable power source to light up LEDs: (E) SSG/TENG array under natural state and (F) SSG/TENG array lights up LEDs.

(G) Power distribution of SSG/TENG arrays excited by impact. Reproduced with permission.<sup>53</sup> Copyright 2019, Elsevier.

(H) Influence of the magnetic field on SSG/TENG performance.

(I) Voltage responds to magnetic fields when a magnet passes over the SSG/TENG.

(J) Voltage-loading forces under different magnetic fields. Reproduced with permission.<sup>54</sup> Copyright 2020, Royal Society of Chemistry.

investigation of the shear stiffening effect and mechanism, an interesting “plastic-elastic-glassy” phase transition process has been proposed in the boron-siloxane polymer system by analyzing the dynamic evolution of B-O dynamic crosslink ligands. In consideration of its unique rate-dependent behavior and numerous modification methods with reinforcement particles, the SSGs have been widely applied in damper controlling, flexible protecting, dynamic sensing, and TENGs.

With the continuous development of multifunctional protective materials, more requirements have been put forward for high-performance anti-impact devices. Owing to the excellent shear stiffening behavior and multifield coupling effect,



the SSGs exhibit great potential in designing next-generation intelligent anti-impact devices, which will make this lightweight flexible polymer play a more important role in the field of personal protection and military security. Undeniably, there are still some challenges in the development of SSGs. Thus far, it is an urgent task to establish precise and reversible relationships between the formulas of raw materials and the final properties of SSG composites. In this case, the controllable performance of SSG composites during the preparation process should be realized. In addition, there is a lack of reports on the structural topology optimization design of SSGs in the existing research. Hence, it is scientifically significant to discover the SSG structures with lighter weights and better anti-impact behavior based on the numerical analysis method. Most important, the detailed shear stiffening mechanism of the SSG is unclear; therefore, quantitative studies on demonstrating the relationship between the inner dynamic B-O ligands and the mechanical properties of the SSG on mesoscopic scale are urgently required. Overall, as a high-performance rate-dependent material, the SSG has broad scientific value and application prospects in the field of intelligent anti-impact devices.

## ACKNOWLEDGMENTS

Financial support from the National Natural Science Foundation of China (grant nos. 11822209, 11972032, and 12072338), the Fundamental Research Funds for the Central Universities (WK2480000007), and Joint Fund of the USTC-National Synchrotron Radiation Laboratory (KY2090000055) are gratefully acknowledged. Thanks to the instrumentation support from engineering practice center of USTC.

## AUTHOR CONTRIBUTIONS

Conceptualization, C.Z. and S.X.; Writing, C.Z.; Resources, S.W. and W.J.; Funding Acquisition, X.G. and S.X.

## DECLARATION OF INTERESTS

The authors declare no competing interests.

## REFERENCES

1. Fernandez, N., Mani, R., Rinaldi, D., Kadam, D., Mosquet, M., Lombois-Burger, H., Cayer-Barrioz, J., Herrmann, H.J., Spencer, N.D., and Isa, L. (2013). Microscopic mechanism for shear thickening of non-Brownian suspensions. *Phys. Rev. Lett.* *111*, 108301.
2. Mari, R., Seto, R., Morris, J.F., and Denn, M.M. (2014). Shear thickening, frictionless and frictional rheologies in non-Brownian suspensions. *J. Rheol. (N.Y. N.Y.)* *58*, 1693–1724.
3. Wang, S., Jiang, W.Q., Jiang, W.F., Ye, F., Mao, Y., Xuan, S.H., and Gong, X.L. (2014). Multifunctional polymer composite with excellent shear stiffening performance and magnetorheological effect. *J. Mater. Chem. C Mater. Opt. Electron. Devices* *2*, 7133–7140.
4. Clavaud, C., Bérut, A., Metzger, B., and Forterre, Y. (2017). Revealing the frictional transition in shear-thickening suspensions. *Proc. Natl. Acad. Sci. USA* *114*, 5147–5152.
5. Peters, I.R., Majumdar, S., and Jaeger, H.M. (2016). Direct observation of dynamic shear jamming in dense suspensions. *Nature* *532*, 214–217.
6. Wang, Y.P., Wang, S., Xu, C.H., Xuan, S.H., Jiang, W.Q., and Gong, X.L. (2016). Dynamic behavior of magnetically responsive shear-stiffening gel under high strain rate. *Compos. Sci. Technol.* *127*, 169–176.
7. Denn, M.M., Morris, J.F., and Bonn, D. (2018). Shear thickening in concentrated suspensions of smooth spheres in Newtonian suspending fluids. *Soft Matter* *14*, 170–184.
8. Jiang, W.F., Gong, X.L., Wang, S., Chen, Q., Zhou, H., Jiang, W.Q., and Xuan, S.H. (2014). Strain rate-induced phase transitions in an impact-hardening polymer composite. *Appl. Phys. Lett.* *104*, 121915.
9. Lee, Y.S., Wetzel, E.D., and Wagner, N.J. (2003). The ballistic impact characteristics of Kevlar (R) woven fabrics impregnated with a colloidal shear thickening fluid. *J. Mater. Sci.* *38*, 2825–2833.
10. Decker, M.J., Halbach, C.J., Nam, C.H., Wagner, N.J., and Wetzel, E.D. (2007). Stab resistance of shear thickening fluid (STF)-treated fabrics. *Compos. Sci. Technol.* *67*, 565–578.
11. Xu, C.H., Wang, Y., Wu, J., Song, S.C., Cao, S.S., Xuan, S.H., Jiang, W.Q., and Gong, X.L. (2017). Anti-impact response of Kevlar sandwich structure with silly putty core. *Compos. Sci. Technol.* *153*, 168–177.
12. Zhao, C.Y., Xu, C.H., Cao, S.S., Xuan, S.H., Jiang, W.Q., and Gong, X.L. (2019). Anti-impact behavior of a novel soft body armor based on shear thickening gel (STG) impregnated Kevlar fabrics. *Smart Mater. Struct.* *28*, 075036.
13. Zhao, C.Y., Wang, Y.P., Cao, S.S., Xuan, S.H., Jiang, W.Q., and Gong, X.L. (2019). Conductive shear thickening gel/Kevlar wearable fabrics: a flexible body armor with mechano-electric coupling ballistic performance. *Compos. Sci. Technol.* *182*, 107782.
14. Neagu, R.C., Bourban, P.E., and Manson, J.A.E. (2009). Micromechanics and damping properties of composites integrating shear thickening fluids. *Compos. Sci. Technol.* *69*, 515–522.
15. Zhou, H., Yan, L.X., Jiang, W.Q., Xuan, S.H., and Gong, X.L. (2016). Shear thickening fluid-based energy-free damper: Design and dynamic characteristics. *J. Intell. Mater. Syst. Struct.* *27*, 208–220.

16. Liang, J., and Zhang, X.H. (2015). Rheological properties of SP in shock transmission application. *J. Mater. Civ. Eng.* *27*, 04014250.
17. Lin, X.G., Guo, F., Du, C.B., and Yu, G.J. (2018). The mechanical properties of a novel STMR damper based on magnetorheological silly putty. *Adv. Mater. Sci. Eng.* *2018*, 2681461.
18. Cheng, X., McCoy, J.H., Israelachvili, J.N., and Cohen, I. (2011). Imaging the microscopic structure of shear thinning and thickening colloidal suspensions. *Science* *333*, 1276–1279.
19. Wagner, N.J., and Brady, J.F. (2009). Shear thickening in colloidal dispersions. *Phys. Today* *62*, 27–32.
20. Brown, E., and Jaeger, H.M. (2014). Shear thickening in concentrated suspensions: phenomenology, mechanisms and relations to jamming. *Rep. Prog. Phys.* *77*, 046602.
21. Li, S., Wang, J., Zhao, S., Cai, W., Wang, Z., and Wang, S. (2017). Giant rheological effect of shear thickening suspension comprising silica nanoparticles with no aggregation. *J. Mater. Sci. Technol.* *33*, 261–265.
22. Egres, R.G., and Wagner, N.J. (2005). The rheology and microstructure of acicular precipitated calcium carbonate colloidal suspensions through the shear thickening transition. *J. Rheol. (N.Y. N.Y.)* *49*, 719–746.
23. Yang, H.G., Li, C.Z., Gu, H.C., and Fang, T.N. (2001). Rheological behavior of titanium dioxide suspensions. *J. Colloid Interface Sci.* *236*, 96–103.
24. Fall, A., Huang, N., Bertrand, F., Ovarlez, G., and Bonn, D. (2008). Shear thickening of cornstarch suspensions as a reentrant jamming transition. *Phys. Rev. Lett.* *100*, 018301.
25. Otsubo, Y., Fujiwara, M., Kouno, M., and Edamura, K. (2007). Shear-thickening flow of suspensions of carbon nanofibers in aqueous PVA solutions. *Rheol. Acta* *46*, 905–912.
26. Chang, L., Friedrich, K., Schlarb, A.K., Tanner, R., and Ye, L. (2011). Shear-thickening behaviour of concentrated polymer dispersions under steady and oscillatory shear. *J. Mater. Sci.* *46*, 339–346.
27. Cao, S.S., Pang, H.M., Zhao, C.Y., Xuan, S.H., and Gong, X.L. (2020). The CNT/PSt-EA/Kevlar composite with excellent ballistic performance. *Compos. Part B Eng.* *185*, 107793.
28. Franks, G.V., Zhou, Z.W., Duin, N.J., and Boger, D.V. (2000). Effect of interparticle forces on shear thickening of oxide suspensions. *J. Rheol. (N.Y. N.Y.)* *44*, 759–779.
29. O'Brien, V.T., and Mackay, M.E. (2000). Stress components and shear thickening of concentrated hard sphere suspensions. *Langmuir* *16*, 7931–7938.
30. Comtet, J., Chatté, G., Niguès, A., Bocquet, L., Siria, A., and Colin, A. (2017). Pairwise frictional profile between particles determines discontinuous shear thickening transition in non-colloidal suspensions. *Nat. Commun.* *8*, 15633.
31. Wyart, M., and Cates, M.E. (2014). Discontinuous shear thickening without inertia in dense non-Brownian suspensions. *Phys. Rev. Lett.* *112*, 098302.
32. Gurgen, S., Kushan, M.C., and Li, W. (2017). Shear thickening fluids in protective applications: a review. *Prog. Polym. Sci.* *75*, 48–72.
33. Ye, Y., Xiao, H., Reaves, K., McCulloch, B., Mike, J.F., and Lutkenhaus, J.L. (2018). Effect of nanorod aspect ratio on shear thickening electrolytes for safety-enhanced batteries. *ACS Appl. Nano Mater.* *1*, 2774–2784.
34. Liu, M., Jian, W.Q., Wang, S., Xuan, S.H., Bai, L.F., Sang, M., and Gong, X.L. (2018). Shear thickening fluid with tunable structural colors. *Smart Mater. Struct.* *27*, 095012.
35. Zhang, X.Z., Li, W.H., and Gong, X.L. (2008). The rheology of shear thickening fluid (STF) and the dynamic performance of an STF-filled damper. *Smart Mater. Struct.* *17*, 035027.
36. Cross, R. (2012). Elastic and viscous properties of silly putty. *Am. J. Physiol.* *80*, 870–875.
37. Wang, Y.P., Gong, X.L., and Xuan, S.H. (2018). Study of low-velocity impact response of sandwich panels with shear-thickening gel cores. *Smart Mater. Struct.* *27*, 065008.
38. Li, X.F., Zhang, D.A., Xiang, K.W., and Huang, G.S. (2014). Synthesis of polyborosiloxane and its reversible physical crosslinks. *RSC Advances* *4*, 32894–32901.
39. Wang, S., Xuan, S., Wang, Y., Xu, C., Mao, Y., Liu, M., Bai, L., Jiang, W., and Gong, X. (2016). Stretchable polyurethane sponge scaffold strengthened shear stiffening polymer and its enhanced safeguarding performance. *ACS Appl. Mater. Interfaces* *8*, 4946–4954.
40. Zhang, X.Z., Li, W.H., and Gong, X.L. (2008). Study on magnetorheological shear thickening fluid. *Smart Mater. Struct.* *17*, 01505.
41. Wang, Y.P., Ding, L., Zhao, C.Y., Wang, S., Xuan, S.H., Jiang, H., and Gong, X.L. (2018). A novel magnetorheological shear-stiffening elastomer with self-healing ability. *Compos. Sci. Technol.* *168*, 303–311.
42. Zhang, S.S., Wang, S., Wang, Y.P., Fan, X.W., Ding, L., Xuan, S.H., and Gong, X.L. (2018). Conductive shear thickening gel/polyurethane sponge: a flexible human motion detection sensor with excellent safeguarding performance. *Compos. Part A Appl. S* *112*, 197–206.
43. D3O home page. <https://www.d3o.com/>.
44. He, Q.Y., Cao, S.S., Wang, Y.P., Xuan, S.H., Wang, P.F., and Gong, X.L. (2018). Impact resistance of shear thickening fluid/Kevlar composite treated with shear-stiffening gel. *Compos. Part A Appl. S* *106*, 82–90.
45. Chang, Z., He, Y.B., Deng, H., Li, X., Wu, S.C., Qiao, Y., Wang, P.F., and Zhou, H.S. (2018). A multifunctional silly-putty nanocomposite spontaneously repairs cathode composite for advanced Li-S batteries. *Adv. Funct. Mater.* *28*, 1804777.
46. Wang, S., Gong, L.P., Shang, Z.J., Ding, L., Yin, G.S., Jiang, W.Q., Gong, X.L., and Xuan, S.H. (2018). Novel safeguarding tactile e-skins for monitoring human motion based on SST/PDMS-AgNW-PET hybrid structures. *Adv. Funct. Mater.* *28*, 1707538.
47. Zhang, S.S., Wang, S., Hu, T., Xuan, S.H., Jiang, H., and Gong, X.L. (2020). Study the safeguarding performance of shear thickening gel by the mechanoluminescence method. *Compos. Part B Eng.* *180*, 107564.
48. Fan, X.W., Wang, S., Zhang, S.S., Wang, Y., and Gong, X.L. (2019). Magnetically sensitive nanocomposites based on the conductive shear-stiffening gel. *J. Mater. Sci.* *54*, 6971–6981.
49. Wang, S., Xuan, S., Liu, M., Bai, L., Zhang, S., Sang, M., Jiang, W., and Gong, X. (2017). Smart wearable Kevlar-based safeguarding electronic textile with excellent sensing performance. *Soft Matter* *13*, 2483–2491.
50. Yuan, F., Wang, S., Zhang, S.S., Wang, Y., Xuan, S.H., and Gong, X.L. (2019). A flexible viscoelastic coupling cable with selfadapted electrical properties and anti-impact performance toward shapeable electronic devices. *J. Mater. Chem. C Mater. Opt. Electron. Devices* *7*, 8412.
51. Wang, S., Xuan, S., Jiang, W., Jiang, W., Yan, L., Mao, Y., Liu, M., and Gong, X. (2015). Rate-dependent and self-healing conductive shear stiffening nanocomposite: a novel safeguarding material with force sensitivity. *J. Mater. Chem. A Mater. Energy Sustain.* *3*, 19790–19799.
52. Boland, C.S., Khan, U., Ryan, G., Barwich, S., Charifou, R., Harvey, A., Backes, C., Li, Z., Ferreira, M.S., Möbius, M.E., et al. (2016). Sensitive electromechanical sensors using viscoelastic graphene-polymer nanocomposites. *Science* *354*, 1257–1260.
53. Wang, S., Ding, L., Wang, Y., and Gong, X.L. (2019). Multifunctional triboelectric nanogenerator towards impact energy harvesting and safeguards. *Nano Energy* *59*, 434–442.
54. Wang, S., Yuan, F., Liu, S., Zhou, J.Y., Xuan, S.H., Wang, Y., and Gong, X.L. (2020). A smart triboelectric nanogenerator with tunable rheological and electrical performance for self-powered multi-sensors. *J. Mater. Chem. C Mater. Opt. Electron. Devices* *8*, 3715–3723.
55. Chen, Y., Pu, X., Liu, M., Kuang, S., Zhang, P., Hua, Q., Cong, Z., Guo, W., Hu, W., and Wang, Z.L. (2019). Shape-adaptive, self-healable triboelectric nanogenerator with enhanced performances by soft solid-solid contact electrification. *ACS Nano* *13*, 8936–8945.
56. Wang, S., Ding, L., Fan, X.W., Jiang, W.F., and Gong, X.L. (2018). A liquid metal-based triboelectric nanogenerator as stretchable electronics for safeguarding and self-powered mechanosensing. *Nano Energy* *53*, 863–870.
57. Seetapan, N., Fuongfuchat, A., Sirikittikul, D., and Limparyoon, N. (2013). Unimodal and bimodal networks of physically crosslinked polyborodimethylsiloxane: viscoelastic and equibiaxial extension behaviors. *J. Polym. Res.* *20*, 183.
58. Tang, M., Wang, W.T., Xu, D.H., and Wang, Z.G. (2016). Synthesis of structure-controlled polyborosiloxanes and investigation on their viscoelastic response to molecular mass of polydimethylsiloxane triggered by both chemical and physical interactions. *Ind. Eng. Chem. Res.* *55*, 12582–12589.

59. Tang, M., Zheng, P., Wang, K.Q., Qin, Y.J., Jiang, Y.Z., Cheng, Y.R., Li, Z., and Wu, L.M. (2019). Autonomous self-healing, self-adhesive, highly conductive composites based on a silver-filled polyborosiloxane/polydimethylsiloxane double-network elastomer. *J. Mater. Chem. A Mater. Energy Sustain.* **7**, 27278–27288.
60. Wu, Q., Xiong, H., Peng, Y., Yang, Y., Kang, J., Huang, G., Ren, X., and Wu, J. (2019). Highly stretchable and self-healing “solid-liquid” elastomer with strain-rate sensing capability. *ACS Appl. Mater. Interfaces* **11**, 19534–19540.
61. Selver, E. (2019). Impact and damage tolerance of shear thickening fluids-impregnated carbon and glass fabric composites. *J. Reinf. Plast. Compos.* **38**, 669–688.
62. Mawkhlieng, U., and Majumdar, A. (2019). Deconstructing the role of shear thickening fluid in enhancing the impact resistance of high-performance fabrics. *Compos. Part B Eng.* **175**, 107167.
63. O’Driscoll, D.P., Vega-Mayoral, V., Harley, I., Boland, C.S., and Coleman, J.N. (2018). Optimising composite viscosity leads to high sensitivity electromechanical sensors. *2D Mater.* **5**, 035042.
64. Ashtiani, M., Hashemabadi, S.H., and Ghaffari, A. (2015). A review on the magnetorheological fluid preparation and stabilization. *J. Magn. Magn. Mater.* **374**, 716–730.
65. Danas, K., Kankanala, S.V., and Triantafyllidis, N. (2012). Experiments and modeling of iron-particle-filled magnetorheological elastomers. *J. Mech. Phys. Solids* **60**, 120–138.
66. Pang, H., Xuan, S., Liu, T., and Gong, X. (2015). Magnetic field dependent electro-conductivity of the graphite doped magnetorheological plastomers. *Soft Matter* **11**, 6893–6902.
67. Qi, S., Fu, J., Xie, Y.P., Li, Y.P., Gan, R.Y., and Yu, M. (2019). Versatile magnetorheological elastomer with 3D printability, switchable mechanics, shape memory, and self-healing capacity. *Compos. Sci. Technol.* **183**, 107817.
68. Golinelli, N., Spaggiari, A., and Dragoni, E. (2017). Mechanical behaviour of magnetic Silly Putty: Viscoelastic and magnetorheological properties. *J. Intell. Mater. Syst. Struct.* **28**, 953–960.
69. Guo, F., Du, C.B., Yu, G.J., and Li, R.P. (2016). The static and dynamic mechanical properties of magnetorheological silly putty. *Adv. Mater. Sci. Eng.* **2016**, 7079698.
70. Liu, B., Du, C.B., and Fu, Y.K. (2019). Factors influencing the rheological properties of MRSP based on the orthogonal experimental design and the impact energy test. *Adv. Mater. Sci. Eng.* **2019**, 2545203.
71. Rogers, S. (2018). Large amplitude oscillatory shear simple to describe, hard to interpret. *Phys. Today* **71**, 34–40.
72. Rudolf, M., Boutelier, D., Rosenau, M., Schreurs, G., and Oncken, O. (2016). Rheological benchmark of silicone oils used for analog modeling of short- and long-term lithospheric deformation. *Tectonophysics* **684**, 12–22.
73. Cross, R. (2012). Elastic properties of plasticine, silly putty, and tennis strings. *Phys. Teach.* **50**, 527–529.
74. Goertz, M.P., Zhu, X.Y., and Houston, J.E. (2009). Temperature dependent relaxation of a “solid-liquid.” *J Polym Sci Pol Physiol.* **47**, 1285–1290.
75. Zinchenko, G.A., Mileshekevich, V.P., and Kozlova, N.V. (1981). Investigation of the synthesis and hydrolytic degradation of polyborodimethylsiloxanes. *Polymer Sci. USSR* **23**, 1421–1429.
76. Liu, Z., Picken, S.J., and Besseling, N.A.M. (2014). Polyborosiloxanes (PBSs), synthetic kinetics, and characterization. *Macromolecules* **47**, 4531–4537.
77. Zhang, D.S., Jiang, N., Chen, X.Y., and He, B.B. (2020). Rheology of crosslinked entangled polymers: Shear stiffening in oscillatory shear. *J. Appl. Polym. Sci.* **137**, 48421.
78. Liu, X.K., Yu, K.J., Fu, Q.Q., and Qian, K. (2019). Shear thickening gel reinforced flexible polyurethane foam and its enhanced properties. *Smart Mater. Struct.* **28**, 055017.
79. Martin, R., Rekondo, A., Ruiz de Luzuriaga, A., Santamaria, A., and Odriozola, I. (2015). Mixing the immiscible: blends of dynamic polymer networks. *RSC Advances* **5**, 17514–17518.
80. Bandaru, A.K., Chavan, V.V., Ahmad, S., Alagirusamy, R., and Bhatnagar, N. (2016). Ballistic impact response of Kevlar (R) reinforced thermoplastic composite armors. *Int. J. Impact Eng.* **89**, 1–13.
81. Monteiro, S.N., Milanezi, T.L., Louro, L.H.L., Lima, E.P., Jr., Braga, F.O., Gomes, A.V., and Drelich, J.W. (2016). Novel ballistic ramie fabric composite competing with Kevlar (TM) fabric in multilayered armor. *Mater. Des.* **96**, 263–269.
82. Taraghi, I., Fereidoon, A., and Taheri-Behrooz, F. (2014). Low-velocity impact response of woven Kevlar/epoxy laminated composites reinforced with multi-walled carbon nanotubes at ambient and low temperatures. *Mater. Des.* **53**, 152–158.
83. Zheng, L., Zhou, H., Gao, C., and Yuan, J. (2012). Hole drilling in ceramics/Kevlar fiber reinforced plastics double-plate composite armor using diamond core drill. *Mater. Des.* **40**, 461–466.
84. Zheng, Y.Y., Fu, M.L., and Wang, C.Y. (2006). Study on the behavior of non-isothermal crystallization and melting of the modified PA6/Kevlar fiber composites. *J. Aeronaut. Mater.* **26**, 51–54.
85. Chen, J., Zhu, G., Yang, W., Jing, Q., Bai, P., Yang, Y., Hou, T.C., and Wang, Z.L. (2013). Harmonic-resonator-based triboelectric nanogenerator as a sustainable power source and a self-powered active vibration sensor. *Adv. Mater.* **25**, 6094–6099.
86. Liu, W., Wang, Z., Wang, G., Liu, G., Chen, J., Pu, X., Xi, Y., Wang, X., Guo, H., Hu, C., and Wang, Z.L. (2019). Integrated charge excitation triboelectric nanogenerator. *Nat. Commun.* **10**, 1426.
87. Zhu, G., Peng, B., Chen, J., Jing, Q., and Wang, Z.L. (2015). Triboelectric nanogenerators as a new energy technology: From fundamentals, devices, to applications. *Nano Energy* **14**, 126–138.